Melting Experiments on Fe-O-H and Fe-H: Evidence for Eutectic Melting in Fe-FeH and Implications for Hydrogen in the Core

Kenta Oka[1], Nagi Ikuta[1], Shoh Tagawa[2], Kei Hirose[2], and Yasuo Ohishi[3]

[1]Univ. Tokyo
[2]Tokyo Institute of Technology
[3]Japan Synchrotron Radiation Research Institute

November 26, 2022

Abstract

We examined liquidus phase relations in Fe-O±H at ˜40 and ˜150 GPa, and in Fe-H at 45 GPa. While it has been speculated that Fe and FeH form continuous solid solution to core pressures, our experiment on Fe-H showed that $FeH_{0.20}$ forms with the hcp structure, different from fcc for stoichiometric FeH, and melts at temperature lower than that for FeH, suggesting eutectic melting between Fe and FeH. It is consistent with the liquidus phase diagram in Fe-O-H, which implies the Fe-FeH binary eutectic liquid composition of $FeH_{0.42}$ at ˜40 GPa. We estimated the outer core liquid composition to be Fe + 2.9–5.2% O + 0.03–0.32% H + 0–3.4% Si + 1.7% S by weight, based on the liquidus phase relations, solid-liquid partitioning, and outer/inner core densities and velocities, indicating that O and either H or Si are important core light elements.

Hosted file

essoar.10511504.1.docx available at https://authorea.com/users/523703/articles/606016-melting-experiments-on-fe-o-h-and-fe-h-evidence-for-eutectic-melting-in-fe-feh-and-implications-for-hydrogen-in-the-core

Melting Experiments on Fe-O-H and Fe-H: Evidence for Eutectic Melting in Fe-FeH and Implications for Hydrogen in the Core

Kenta Oka[1], Nagi Ikuta[1], Shoh Tagawa[1,2], Kei Hirose[1,2], and Yasuo Ohishi[3]

[1]Department of Earth and Planetary Science, The University of Tokyo, Bunkyo, Tokyo, Japan
[2]Earth-Life Science Institute, Tokyo Institute of Technology, Meguro, Tokyo, Japan
[3]Japan Synchrotron Radiation Research Institute, SPring-8, Sayo, Hyogo, Japan

Key Points:

- We examined the liquidus phase relations and solid/liquid partitioning in the Fe-O±H and Fe-H systems at ~40 GPa and ~150 GPa.
- Eutectic melting between Fe and FeH is indicated from the phase relations and melting temperature in Fe-O-H and Fe-H.
- The outer core may include 2.9–5.2 wt% O, 0.03–0.32 wt% H, 0–3.4 wt% Si, and 1.7 wt% S.

Abstract We examined liquidus phase relations in Fe-O±H at ~40 and ~150 GPa, and in Fe-H at 45 GPa. While it has been speculated that Fe and FeH form continuous solid solution to core pressures, our experiment on Fe-H showed that $FeH_{0.20}$ forms with the hcp structure, different from fcc for stoichiometric FeH, and melts at temperature lower than that for FeH, suggesting eutectic melting between Fe and FeH. It is consistent with the liquidus phase diagram in Fe-O-H, which implies the Fe-FeH binary eutectic liquid composition of $FeH_{0.42}$ at ~40 GPa. We estimated the outer core liquid composition to be Fe + 2.9–5.2% O + 0.03–0.32% H + 0–3.4% Si + 1.7% S by weight, based on the liquidus phase relations, solid-liquid partitioning, and outer/inner core densities and velocities, indicating that O and either H or Si are important core light elements.

Plain Language Summary We have investigated the melting phase relations in the Fe-O±H and Fe-H systems at high pressures in a laser-heated diamond-anvil cell. The solid-liquid partition coefficient of H was also determined. While it is known that Fe and stoichiometric FeH form continuous solid solution at least to ~20 GPa, our experiments on the Fe-O-H ternary and Fe-H binary systems performed at ~40 GPa consistently suggested eutectic melting between Fe and FeH with eutectic liquid composition of $FeH_{0.42}$. We explored the possible range of the Earth's liquid core

composition, which should be 1) within the liquidus field of Fe to crystallize the dense inner core, 2) compatible with seismological observations of the outer core, and 3) in chemically equilibrium with the inner core solid that explains the observed density and velocities. The results indicate that the outer core is rich in O and either H or Si, supporting the delivery of a large amount of water to the Earth found in recent planet formation theories and its sequestration into the metallic core that is also inferred from metal-silicate partitioning data.

1. Introduction

The Earth's core should contain more than one light impurity elements (see recent reviews by Li & Fei, 2014 and Hirose et al., 2021). Both O and H can be important core light elements because the density and sound velocity observed in the outer core are compatible with the presence of O (Badro et al., 2014) and H (Umemoto & Hirose, 2015, 2020). Recent planet formation models suggested that 10 to 100 times ocean mass of water may have been brought to the Earth during its accretion (e.g., Raymond et al., 2007; Walsh et al., 2011). The chemical reaction of solar-nebula-type H-rich proto-atmosphere with a magma ocean could have been another source of water (Ikoma & Genda, 2006; Olson & Sharp, 2019). It is likely that most of H_2O was once dissolved into a magma ocean, and H and O were incorporated into core-forming metals during their segregation from silicate (Tagawa et al., 2021; Li et al., 2020; Yuan & Steinle-Neumann, 2020).

Liquidus phase relations of Fe alloy systems, in particular the liquidus field of Fe (a compositional range of liquids that first crystallize Fe), constrain the outer core composition (e.g., Yokoo et al., 2019; Hasegawa et al., 2021; Sakai & Hirose, 2021). When O and H are two major core light elements, the liquid core should not crystallize FeO nor FeH but Fe at the inner core boundary (ICB), otherwise the denser solid inner core is not formed. In order to understand the liquidus phase relations in the Fe-O-H system, the knowledge on the relevant binary systems is helpful. Previous high-pressure experiments demonstrated that O concentration in the Fe-FeO eutectic liquid increases with increasing pressure (Morard et al., 2017; Oka et al., 2019). The recent study by Oka and others based on experiments to 204 GPa estimated 15 wt% O in the Fe-FeO binary eutectic liquid at ICB. On the other hand, earlier high-pressure melting experiments on the Fe(±Ni)-H system were limited to 20 GPa (Sakamaki et al., 2009; Imai, 2013; Shibazaki et al., 2014) because of a technical difficulty in dealing with hydrogen. Fukai (1992) speculated continuous solid solution between Fe and

stoichiometric FeH to megabar pressure, but it has been verified only to ~20 GPa (Imai, 2013; Shibazaki et al., 2014).

In this study, we have carried out melting experiments on the Fe-O±H and Fe-H systems at ~40 GPa and ~150 GPa. Our results on Fe-O-H suggest that Fe-FeH is an eutectic system, which contradicts the phase diagram supposed by Fukai (1992) but is supported by our experiment on Fe-H alloy. Our findings of 1) eutectic melting between Fe and FeH, 2) liquidus phase relations in the Fe-O-H system, and 3) the solid-liquid partitioning of H help to constrain concentrations of O, H, and other light elements in the outer core.

2. Results

We have examined the melting phase relations in the Fe-O±H and Fe-H systems on the basis of high-pressure and -temperature (*P-T*) experiments using laser-heated diamond-anvil cell (DAC) techniques, combined with in-situ synchrotron X-ray diffraction (XRD) measurements and ex-situ textural and compositional characterizations using electron microprobes (see Experimental Methods in the Supporting Information).

2.1. Melting in Fe-O±H

A total of six separate melting experiments were carried out in the Fe-O±H system at ~40 GPa and ~150 GPa (runs #A1–A6 in Table S1). For all runs, we performed synchrotron XRD measurements and subsequent microprobe observations on recovered samples. In run #A4, while the intense peaks from hcp Fe were present before heating, they were almost lost and alternatively a diffuse signal characteristic of liquid was observed around 12 degrees of two-theta angle upon heating to 2370 K (Figure 1a). Upon quenching temperature, the peaks of fcc FeH_x (x = 0.31) appeared from the liquid portion. The XRD pattern obtained at ~12 μm away from the center of a laser-heated spot included strong peaks from rhombohedrally-distorted B1 FeO and hcp $FeH_{0.24}$.

This sample was recovered from a DAC, and in its cross section, there was a chemically homogeneous area with a non-stoichiometric composition at the center, which represents a quenched liquid (Figures 2a, b). The earlier DAC experiments by Hirose et al. (2019) and Tagawa et al. (2021) demonstrated that the H content in FeH_x crystals formed from liquid upon quenching temperature closely represents that of Fe-H liquid. We therefore consider that Fe-O-H liquids in the present experiments were fully

quenched into a mixture of solid FeH_x and FeO. The proportion of FeO was obtained from the EPMA analysis of O concentration in the quenched liquid. The remaining phase proportion of FeH_x and its H concentration x that was estimated from its lattice volume in XRD patterns give 0.49 wt% H in the Fe-O-H liquid (Table S1). Next to the liquid pool, electron microprobe images showed a couple of single-phase layers of Fe and FeO (Figures 2a, b). According to the XRD observations, the Fe layer had been solid $FeH_{0.24}$ (Fe + 0.43 wt% H) before it lost hydrogen during decompression (Figure 1a). The partition coefficient of H between solid Fe and liquid, D_H (solid/liquid), was 0.89 on weight basis. The liquid was in direct contact with the FeO layer or in some place with the $FeH_{0.24}$ layer, indicating that both FeO and $FeH_{0.24}$ are the liquidus phases of the Fe-O-H liquid formed in run #A4. The outside of these liquidus phase layers was not melted. Runs #A1–A3 were carried out around 40 GPa in a similar manner with changing the Fe/H_2O ratio in the starting materials (Table S1). These liquids included 0.1–0.4 wt% C except 1.7 wt% C in run #A1.

In runs #A5 and #A6 performed at ~150 GPa, liquids were crystallized into the hcp phase upon quenching temperature to 300 K, which included minimal amounts of H (<0.04 wt%) (Table S1). The EPMA data showed 10.4–13.0 wt% O and 0.9–3.7 wt% C in quenched liquids, indicating they were Fe-O±C liquids. The liquid Fe-13.0wt%O-0.9wt%C obtained in run #A5 coexisted with solid Fe, giving the lower bound for O concentration in the Fe-FeO binary eutectic liquid at 147 GPa (Figure S1). It helps to constrain the change in the eutectic liquid composition in the Fe-FeO system with increasing pressure, which was previously estimated only with a single datum point above 50 GPa in Oka et al. (2019).

2.2. Melting in Fe-H

Melting experiment was carried out also on the Fe-FeH binary system at 45 GPa (run #B, Table S2) (see Experimental Methods in the Supporting Information). Non-stoichiometric hcp $FeH_{0.30}$ was synthesized by heating to <1000 K at 10 GPa (Figure 1b). The excess molecular H_2 in a sample chamber was lost to a neighboring rhenium gasket to form Re-H alloy upon compression to 23 GPa at room temperature (Scheler et al., 2011). After further compression, we melted this sample by heating to 1900 K for 80 sec at 45 GPa. The hcp 002, 101, and 102 peaks were observed in the XRD pattern during heating, and the presence of liquid was confirmed when quenching temperature by the appearance of the new hcp 100 and 110 peaks and of the hcp 002, 101 and 102 additional spot peaks in the 2D XRD image. We found the H content in

liquid to be $FeH_{0.26}$ from these hcp peaks that emerged upon temperature quench (Figure 1b). The solid phase that coexisted with liquid was hcp $FeH_{0.20}$ based on spot peaks that were present during heating. These results show the solid/liquid partition coefficient of H, D_H = 0.77 on weight basis. Carbon contamination should have been minor in this experiment because the sample was heated only to 1900 K, much less than in other melting experiments on Fe-O-H.

3. Discussion

3.1. Eutectic Melting in Fe-FeH and the Liquidus Phase Relations in Fe-O-H

The high-pressure phase relations in the Fe-H system have been speculated by Fukai (1992), suggesting 1) continuous solid solution between Fe and FeH and 2) an eutectic composition with FeH_x ($x > 1$). The multi-anvil experiments by Imai (2013) and Shibazaki et al. (2014) reported the melting and subsolidus phase relations in the Fe-FeH(±Ni) system to 15–20 GPa, which are consistent with the phase diagram supposed by Fukai (1992). In contrast, in the present experiment (run #B), melting occurred by heating to 1900 K at 45 GPa, lower than the melting point of 2100 K for stoichiometric FeH (Tagawa, Helffrich et al., 2022) (note that if Fe and FeH form continuous solid solution, the solidus temperature of $FeH_{0.20\text{-}0.30}$ should be closer to the melting point of pure Fe than that of FeH). In addition, we found $FeH_{0.20}$ with the hcp structure at this *P-T* condition, which is different from the fcc structure for FeH (Kato et al., 2020; Thompson et al., 2018; Tagawa, Gomi et al., 2022). It indicates a gap in solid solution between Fe and FeH. These suggest eutectic (not peritectic) melting between the H-poor hcp and H-rich fcc phases in the Fe-FeH system. The presence of the gap in solid solution between hcp Fe and fcc FeH and the resulting eutectic melting are likely to be hold to Earth's inner core conditions (Tagawa, Helffrich et al., 2022).

The compositions of liquids obtained at ~40 GPa in runs #A1–A4 and #B are plotted in the Fe-O-H ternary diagram (Figure 3a). The liquid compositions found in runs #A2 and #A3 should be within the liquidus field of FeO, and that in run #A4 is on the Fe + FeO cotectic line (showing the liquid compositions coexisting with both Fe and FeO). Considering the eutectic point in the Fe-FeO binary (Figure S1), the position of the Fe + FeO cotectic line is tightly constrained. Figure 3a illustrates the liquidus phase relations in the Fe-O-H system. The liquidus field of FeO extends close to the Fe-FeH side, and the ternary peritectic (unlikely eutectic) point should be located at the H-rich portion of the phase diagram. It suggests the presence of the Fe-FeH binary eutectic point at $FeH_{0.42}$ (Fe + 0.75 wt% H). It includes more hydrogen than the liquid $FeH_{0.26}$ obtained

169 at 1900 K in run #B, suggesting that the Fe-FeH binary eutectic temperature is
170 somewhat lower than 1900 K at 45 GPa.

171 The Fe-FeH binary eutectic liquid composition may change little with increasing
172 pressure because the high *P*-*T* experiments performed by Tagawa, Helffrich et al. (2022)
173 showed that the temperature/pressure slope of the melting curve of stoichiometric FeH
174 is similar to that of Fe at >40 GPa. On the other hand, the present results on the Fe-FeO
175 system as well as earlier experiments (Seagle et al., 2008; Oka et al., 2019) and
176 thermodynamic calculations (Komabayashi, 2014) demonstrate that O concentration in
177 the Fe-FeO binary eutectic liquid increases to 15 wt% with increasing pressure to 330
178 GPa. The Fe-O±C liquids obtained in runs #A5 and #A6 verify the pressure evolution of
179 the Fe-FeO eutectic liquid composition (the composition of liquid that coexists with
180 both Fe and FeO) in the presence of <1 wt% and ~3 wt% C, respectively (Figure S1).
181 By taking the positions of the Fe-FeO and Fe-FeH binary eutectic points into account,
182 we suppose the Fe-O-H ternary liquidus phase relations at the ICB pressure in Figure
183 3b.

184 **3.2. Possible Outer Core Liquid Composition**

185 Since the outer core crystallizes the dense inner core at the ICB, the liquid composition
186 should be within the liquidus field of Fe at 330 GPa (Figure 3b). It has been
187 demonstrated by earlier experiments on ternary Fe alloy systems containing two light
188 elements—Fe-Si-S (Tateno et al., 2018), Fe-S-O (Yokoo et al., 2019), Fe-Si-C
189 (Hasegawa et al., 2021), and Fe-C-O (Sakai & Hirose, 2021)—that the ternary eutectic
190 point is located close to the tie line between the eutectic points in relevant binary
191 systems; in other words, the liquidus field of Fe (such as a colored area in Figure 3b) in
192 these ternary systems can be approximated by linear interpolation between the eutectic
193 liquid compositions in relevant binary systems. This may be extended to the
194 Fe-O-H-Si-S system that we consider for the liquid outer core; the liquidus field of Fe
195 could be estimated from the four relevant binary eutectic compositions at 330 GPa; Fe
196 with 15 wt% O (Figure S1), 0.75 wt% H (Figure 3b), 8 wt% Si (Hasegawa et al., 2021),
197 or 5 wt% S (Mori et al., 2017).

198 We estimate the possible range of the outer core liquid composition based on three
199 independent constraints (Hirose et al., 2021). First, 1) it must account for the density
200 and P-wave velocity observed in the outer core (Umemoto & Hirose, 2020). We first
201 consider T_{ICB} = 5800 K and 6280 K, which correspond to T_{360GPa} = 6000 K and 6500 K,
202 respectively, when assuming isentropic temperature profiles with Grüneisen parameter γ

= 1.5 (Vočadlo et al., 2003); these are the conditions at which the possible inner core composition was examined by Wang et al. (2021). Also, 2) the liquid core composition should be within the liquidus field of Fe in the Fe-O-H-Si±1.7wt%S system at the ICB pressure. Geochemical and cosmochemical estimates have consistently proposed ~2 wt% S in the core (Dreibus & Palme, 1996; McDonough, 2014), and here we adopt 0 or 1.7 wt% S in the outer core according to Dreibus & Palme. The colored portions in Figures 4a–d indicate O, H, and Si concentrations in liquids Fe-Ni-O-H-Si±1.7wt%S (Fe/Ni =16 by weight), which meet these two constraints from 1) the outer core density and velocity and 2) the liquidus phase diagram at 330 GPa.

In addition, 3) the third constraint is from the possible inner core solid composition that was estimated in Fe-Si-S(-C) by Li et al. (2018) and in Fe-H-Si by Wang et al. (2021), which explains the observed density, P-wave and S-wave velocities (Dziewonski & Anderson, 1981; Kennett et al., 1995). Their calculations of $Fe_{64-y}Si_y$ (y = 0, 4, and 8) and $Fe_{60}Si_4H_z$ (z = 1, 2, 4, and 8) alloys demonstrated that the density (ρ), P-wave (V_P) and S-wave velocities (V_S) of Fe alloys are written as; $\rho = -0.105y - 0.039z + 13.639(5)$, $V_P = -0.001y - 0.034z + 11.559(128)$, and $V_S = -0.061y - 0.053z + 4.108(154)$ at T_{360GPa} = 6500 K, and $\rho = -0.104y - 0.038z + 13.682(48)$, $V_P = 0.001y - 0.019z + 11.619(110)$, and $V_S = -0.060y - 0.033z + 4.229(140)$ at T_{360GPa} = 6000 K. The inner core may include 1.4 wt% S, which is calculated from the 1.7 wt% S in the outer core and the solid/liquid partition coefficient of S, D_S = 0.8 by weight at 330 GPa (Alfè et al., 2002; Yokoo et al., 2019). Since Wang et al. (2021) mentioned that the effects of S and Si on the density and sound velocities are similar to each other, we consider that the effect of S is equivalent to that of Si. O is not partitioned into solid Fe and thus not considered in the inner core (Alfè et al., 2002; Ozawa et al., 2010). With these relations, we obtain the possible ranges of the inner core composition in the Fe-H-Si±1.4wt%S system, depending on temperature. It gives the liquid outer core composition based on the solid/liquid partition coefficients D_H = 0.89 (from run #A-4 in this study) and D_{Si} = 1.0 by weight (Alfè et al., 2002; Kuwayama & Hirose, 2004). The D_H = 0.77–0.89 obtained in this study at 39–45 GPa is slightly higher than 0.72–0.74 reported by earlier multi-anvil experiments at 15–20 GPa (Imai, 2013). The compositional ranges of liquids in chemical equilibrium with the possible inner core solid are illustrated by areas enclosed by black lines in Figures 4a–d.

The overlap between the colored area (constrained by the outer core density and velocity and by the liquidus field of Fe) and the black enclosed area (constrained by the inner core density and velocities) in Figures 4a–d indicates the possible compositional

range for the liquid outer core. It becomes smaller with 1.7 and 1.4 wt% S respectively in the outer and inner core than in S-free cases. Possible liquid compositions are not found in the Fe-O-H-Si-1.7wt%S system when T_{ICB} = 5800 K (T_{360GPa} = 6000 K) (Figure 4c). If T_{ICB} = 6280 K (T_{360GPa} = 6500 K), the outer core may include 2.9–5.2 wt% O, 0.03–0.32 wt% H, and 0–3.4 wt% Si and in addition to 1.7 wt% S. Furthermore, with T_{ICB} of ~6000 K, the H-rich liquid core with ~0.3 wt% H and ~3 wt% O in addition to 1.7 wt% S and minimal Si satisfies the seismological and liquidus-phase constraints considered here (Figures 4c, d). It suggests that ~1 wt% H_2O in the bulk Earth, corresponding to about 50 ocean mass of water, is sequestrated in the core (Tagawa et al., 2021; Li et al., 2020; Yuan & Steinle-Neumann, 2020). It is supported by recent planet formation theories that a large amount of water was brought to the Earth during its accretion (Raymond et al., 2007; Walsh et al., 2011). The range of the O content is still consistent with the recent estimate of <3.8 wt% O in the outer core to explain the density jump across the ICB, which was based on the experimentally-determined equations of state of liquid and solid Fe (Kuwayama et al., 2020; Dewaele et al., 2006). Indeed, ~0.2 wt.% C could be also present in the core (Fischer et al., 2020), but it hardly decreases the present estimates of the core inventories of other light elements.

The T_{ICB} = 6000–6280 K, however, corresponds to about 4400–4600 K at the CMB when γ = 1.5 (Vočadlo et al., 2003). It is much higher than the solidus temperatures of the pyrolitic and chondritic mantle materials at 135 GPa (Fiquet et al., 2010; Andrault et al., 2011; Nomura et al., 2014; Kim et al., 2020). It could therefore lead to extensive melting in the lowermost mantle at present, but seismology reveals the presence of partial melts only locally at ultralow velocity zones above the CMB. It is necessary to better constrain the core temperature to further explore the possible core composition (Hirose et al., 2021).

4. Conclusions

We obtained the liquidus phase relations in the Fe-O-H ternary and Fe-H binary systems at ~40 GPa. While earlier studies reported that Fe and stoichiometric FeH form continuous solid solution below ~20 GPa (Sakamaki et al., 2009; Imai, 2013; Shibazaki et al., 2014), our results at ~40 GPa indicate eutectic melting between Fe and FeH from the observations that 1) $FeH_{0.20}$ was formed with the hcp structure, different from fcc for stoichiometric FeH, suggesting a miscibility gap between the H-poor hcp and H-rich fcc phases in Fe-FeH, 2) the liquidus temperature of $FeH_{0.26}$ is 1900 K, lower than the melting temperature of FeH (Tagawa, Helffrich et al., 2022), and 3) melting phase

relations in the Fe-O-H ternary require the eutectic point in the Fe-FeH system. The Fe-FeH eutectic liquid composition is found to be $FeH_{0.42}$ (Fe + 0.75 wt% H) at this pressure. The pressure effect on the Fe-FeH eutectic liquid composition is likely to be small because the temperature/pressure slope of the melting curve of FeH is comparable to that of Fe (Tagawa, Helffrich et al., 2022). On the other hand, the present study combined with earlier experiments demonstrates that O concentration in the Fe-FeO binary eutectic liquid increases to 15 wt% at 330 GPa. These allow us to extrapolate the liquidus phase relations in the Fe-O-H system to 330 GPa.

We estimated the possible range of the outer core liquid composition to be Fe + 2.9–5.2 wt% O + 0.03–0.32 wt% H + 0–3.4 wt% Si + 1.7 wt% S when T_{ICB} = 6280 K, based on constraints from 1) the liquidus field of Fe (in order to crystallize the dense inner core), 2) the outer core density and velocity, and 3) the inner core density and velocities (the outer core composition is calculated from that of the inner core using the solid-liquid partition coefficients of light elements at ICB conditions). If T_{ICB} is ~6000 K, the outer core is enriched in both O and H, supporting recent arguments on the delivery of a large amount of water to the growing Earth and its incorporation into core metals for the most part.

Data Availability Statement

Datasets for this research are found in Tables S1, S2, and Dataset S1 available online (from https://doi.org/10.5281/zenodo.6508681).

Acknowledgments

We thank K. Yonemitsu for sample analyses with FIB, EDS, and FE-EPMA. Comments from anonymous reviewers were helpful to improve the manuscript. This work was supported by the JSPS research grants 16H06285 and 21H04968 to K.H. XRD measurements were performed at BL10XU, SPring-8 (proposals no. 2019A0072, 2019B0072, and 2021B0181).

References

Alfè, D., Gillan, M. J., & Price, G. D. (2002). Composition and temperature of the earth's core constrained by combining ab initio calculations and seismic data. *Earth and Planetary Science Letters*, *195*, 91–98. https://doi.org/10.1016/S0012-821X(01)00568-4

Andrault, D., Bolfan-Casanova, N., Nigro, G. Lo, Bouhifd, M. A., Garbarino, G., & Mezouar, M. (2011). Solidus and liquidus profiles of chondritic mantle: implication for melting of the Earth across its history. *Earth and Planetary Science Letters*, *304*, 251–259. https://doi.org/10.1016/j.epsl.2011.02.006

Badro, J., Cote, A. S., & Brodholt, J. P. (2014). A seismologically consistent compositional model of Earth's core. *Proceedings of the National Academy of Science of the United States of America*, *111*, 7542–7545. https://doi.org/10.1073/pnas.1316708111

Dreibus, G., & Palme, H. (1996). Cosmochemical constraints on the sulfur content in the Earth's core. *Geochimica et Cosmochimica Acta*, *60*, 1125–1130. https://doi.org/10.1016/0016-7037(96)00028-2

Dziewonski, A. M., & Anderson, D. L. (1981). Preliminary reference Earth model. *Physics of the Earth and Planetary Interiors*, *25*, 297–356. https://doi.org/10.1016/0031-9201(81)90046-7

Fukai, Y. (1992). Some properties of the Fe-H system at high pressures and temperatures, and their implications for the Earth's core. In Y. Syono, M.H. Manghnani (Eds.), *High-pressure research: applications to Earth and planetary sciences* (Vol. 67, pp. 373–385). https://doi.org/10.1029/GM067p0373

Fischer, R. A., Cottrell, E., Hauri, E., Lee, K. K. M., & Le Voyer, M. (2020). The carbon content of Earth and its core. *Proceedings of the National Academy of Sciences of the United States of America*, *117*, 8743–8749. https://doi.org/10.1073/pnas.1919930117

Fiquet, G., Auzende, A. L., Siebert, J., Corgne, A., Bureau, H., Ozawa, H., & Garbarino, G. (2010). Melting of peridotite to 140 gigapascals. *Science*, *329*, 1516–1518. https://doi.org/10.1126/science.1192448

Hasegawa, M., Hirose, K., Oka, K., & Ohishi, Y. (2021). Liquidus phase relations and solid-liquid partitioning in the Fe-Si-C system under core pressures. *Geophysical Research Letters*, *48*, e2021GL092681. https://doi.org/10.1029/2021GL092681

Hirose, K., Wood, B., & Vočadlo, L. (2021). Light elements in the Earth's core. *Nature Reviews Earth & Environment*, *2*, 645–658. https://doi.org/10.1038/s43017-021-00203-6

Ikoma, M., & Genda, H. (2006). Constraints on the mass of a habitable planet with water of nebular origin. *The Astrophysical Journal*, *648*, 696. https://doi.org/10.1086/505780

Imai, T. (2013). *Crystal/melt partitioning under deep mantle conditions and melting phase relation in the system Fe-FeH* (PhD thesis). Tokyo Institute of Technology

Kato, C., Umemoto, K., Ohta, K., Tagawa, S., Hirose, K., & Ohishi, Y. (2020). Stability of fcc phase FeH to 137 GPa. *American Mineralogist*, *105*, 917–921. https://doi.org/10.2138/am-2020-7153

Kennett, B. L. N., Engdahl, E. R., & Buland, R. (1995). Constraints on seismic velocities in the Earth from traveltimes. *Geophysical Journal International*, *122*, 108–124. https://doi.org/10.1111/j.1365-246X.1995.tb03540.x

Kim, T., Ko, B., Greenberg, E., Prakapenka, V., Shim, S. H., & Lee, Y. (2020). Low melting temperature of anhydrous mantle materials at the core-mantle boundary. *Geophysical Research Letter*s, *47*, 1–10. https://doi.org/10.1029/2020GL089345

Komabayashi, T. (2014). Thermodynamics of melting relations in the system Fe-FeO at high pressure: implications for oxygen in the Earth's core. *Journal of Geophysical Research: Solid Earth*, *119*, 4164–4177. https://doi.org/10.1002/2014JB010980

Komabayashi, T., Fei, Y., Meng, Y., & Prakapenka, V. (2009). In-situ X-ray diffraction measurements of the γ-ε transition boundary of iron in an internally-heated diamond anvil cell. *Earth and Planetary Science Letters*, *282*, 252–257. https://doi.org/10.1016/j.epsl.2009.03.025

Kuwayama, Y., & Hirose, K. (2004). Phase relations in the system Fe-FeSi at 21 GPa. *American Mineralogist*, *89*, 273–276. https://doi.org/10.2138/am-2004-2-303

Kuwayama, Y., Morard, G., Nakajima, Y., Hirose, K., Baron, A. Q. R., Kawaguchi, S. I., et al. (2020). Equation of state of liquid iron under extreme conditions. *Physical Review Letters*, *124*, 165701. https://doi.org/10.1103/PhysRevLett.124.165701

Li, J., & Fei, Y. (2014). Experimental constraints on core composition. In *Treatise on geochemistry* (2nd ed., Vol. 3, pp. 527−557). Amsterdam. Elsevier. https://doi.org/10.1016/b978-0-08-095975-7.00214-x

Li, Y., Vočadlo, & L., Brodholt, J. P. (2018). The elastic properties of hcp-Fe alloys under the conditions of the Earth's inner core. *Earth and Planetary Science Letters*, *493*, 118–127. https://doi.org/10.1016/j.epsl.2018.04.013

Li, Y., Vočadlo, L., Sun, T., & Brodholt, J. P. (2020). The Earth's core as a reservoir of water. *Nature Geoscience*, *13*, 453–458. https://doi.org/10.1038/s41561-020-0578-1

McDonough, W. F. (2014). Compositional model for the Earth's core. In *Treatise on geochemistry* (2nd ed., Vol. 3, pp. 559–577). Amsterdam. Elsevier. https://doi.org/10.1016/B978-0-08-095975-7.00215-1

Morard, G., Andrault, D., Antonangeli, D., Nakajima, Y., Auzende, A. L., Boulard, E., et al. (2017). Fe–FeO and Fe–Fe_3C melting relations at Earth's core–mantle boundary conditions: implications for a volatile-rich or oxygen-rich core. *Earth and Planetary Science Letters*, *473*, 94–103. https://doi.org/10.1016/j.epsl.2017.05.024

Mori, Y., Ozawa, H., Hirose, K., Sinmyo, R., Tateno, S., Morard, G., & Ohishi, Y. (2017). Melting experiments on Fe–Fe_3S system to 254 GPa. *Earth and Planetary Science Letters*, *464*, 135–141. https://doi.org/10.1016/j.epsl.2017.02.021

Nomura, R., Hirose, K., Uesugi, K., Ohishi, Y., Tsuchiyama, A., Miyake, A., & Ueno, Y. (2014). Low core-mantle boundary temperature inferred from the solidus of pyrolite. *Science*, *343*, 522–525. https://doi.org/10.1126/science.1248186

Oka, K., Hirose, K., Tagawa, S., Kidokoro, Y., Nakajima, Y., Kuwayama, Y., et al. (2019). Melting in the Fe-FeO system to 204 GPa: implications for oxygen in Earth's core. *American Mineralogist*, *104*, 1603–1607. https://doi.org/10.2138/am-2019-7081

Olson, P. L., & Sharp, Z.D. (2019). Nebular atmosphere to magma ocean: a model for volatile capture during Earth accretion. *Physics of the Earth and Planetary Interiors*, *294*, 106294. https://doi.org/10.1016/j.pepi.2019.106294

Ozawa, H., Hirose, K., Tateno, S., Sata, N., & Ohishi, Y. (2010). Phase transition boundary between B1 and B8 structures of FeO up to 210GPa. *Physics of the Earth and Planetary Interiors*, *179*, 157–163. https://doi.org/10.1016/j.pepi.2009.11.005

Raymond, S. N., Quinn, T., & Lunine, J. I. (2007). High-resolution simulations of the final assembly of Earth-like planets. 2. Water delivery and planetary habitability. *Astrobiology*, *7*, 66–84. https://doi.org/10.1089/ast.2006.06-0126.

Sakai, F., & Hirose, K. (2021). Melting experiments on the Fe-C-O ternary system under core pressures. JpGU Meeting Abstract

Sakamaki, K., Takahashi, E., Nakajima, Y., Nishihara, Y., Funakoshi, K., Suzuki, T., & Fukai, Y. (2009). Melting phase relation of FeH_X up to 20 GPa: implication for the temperature of the Earth's core. *Physics of the Earth and Planetary Interiors*, *174*, 192–201. https://doi.org/10.1016/j.pepi.2008.05.017

Seagle, C. T., Heinz, D. L., Campbell, A. J., Prakapenka, V. B., & Wanless, S. T. (2008). Melting and thermal expansion in the Fe-FeO system at high pressure. *Earth and Planetary Science Letters*, *265*, 655–665. https://doi.org/10.1016/j.epsl.2007.11.004

Scheler, T., Degtyareva, O., & Gregoryanz, E. (2011). On the effects of high temperature and high pressure on the hydrogen solubility in rhenium. *Journal of Chemical Physics*, *135*, 214501. https://doi.org/10.1063/1.3652863

Shibazaki, Y., Terasaki, H., Ohtani, E., Tateyama, R., Nishida, K., Funakoshi, K., & Higo, Y. (2014). High-pressure and high-temperature phase diagram for $Fe_{0.9}Ni_{0.1}$-H alloy. *Physics of the Earth and Planetary Interiors*, *228*, 192–201. https://doi.org/10.1016/j.pepi.2013.12.013

Stixrude, L. (2012). Structure of iron to 1 Gbar and 40 000 K. *Physical Review Letters*, *108*, 055505. https://doi.org/10.1103/PhysRevLett.108.055505

Tagawa, S., Sakamoto, N., Hirose, K., Yokoo, S., Hernlund, J., Ohishi, Y., & Yurimoto, H. (2021). Experimental evidence for hydrogen incorporation into Earth's core. *Nature Communications*, *12*, 2588. https://doi.org/10.1038/s41467-021-22035-0

Tagawa, S., Gomi, H., Hirose, K., & Ohishi, Y. (2022). High-temperature equation of state of FeH: implications for hydrogen in Earth's inner core. *Geophysical Research Letter*s, *49*, e2021GL096260. https://doi. org/10.1029/2021GL096260

Tagawa, S., Helffrich, G., Hirose, K., Ohishi, Y. (2022). High-Pressure melting curve of FeH: implications for eutectic melting between Fe and non-magnetic FeH. *Earth and Space Science Open Archive*. https://www.essoar.org/doi/abs/10.1002/essoar.10510818.1

Tateno, S., Hirose, K., Sinmyo, R., Morard, G., Hirao, N., & Ohishi, Y. (2018). Melting experiments on Fe–Si–S alloys to core pressures: silicon in the core? *American Mineralogist*, *103*, 742–748. https://doi.org/10.2138/am-2018-6299

Thompson, E. C., Davis, A. H., Bi, W., Zhao, J., Alp, E. E., Zhang, D., et al. (2018). High-pressure geophysical properties of fcc phase FeH_X. *Geochemistry, Geophysics, Geosystems*, *19*, 305–314. https://doi.org/10.1002/2017GC007168

Umemoto, K., & Hirose, K. (2015). Liquid iron-hydrogen alloys at outer core conditions by first-principles calculations. *Geophysical Research Letters*, *42*, 7513–7520. https://doi.org/10.1002/2015GL065899

Umemoto, K., & Hirose, K. (2020). Chemical compositions of the outer core examined by first principles calculations. *Earth and Planetary Science Letters*, *531*, 116009. https://doi.org/10.1016/j.epsl.2019.116009

Vočadlo, L., Alfè, D., Gillan, M. J., & Price, G. D. (2003). The properties of iron under core conditions from first principles calculations. *Physics of the Earth and Planetary Interiors*, *140*, 101–125. https://doi.org/10.1016/j.pepi.2003.08.001

Walsh, K. J., Morbidelli, A., Raymond, S. N., O'brien, D. P., & Mandell, A. M. (2011). A low mass for Mars from Jupiter's early gas-driven migration. *Nature*, *475*, 206–209. https://doi.org/10.1038/nature10201

Wang, W., Li, Y., Brodholt, J. P., Vočadlo, L., Walter, M. J., & Wu, Z. (2021). Strong shear softening induced by superionic hydrogen in Earth's inner core. *Earth and Planetary Science Letters*, *568*, 117014. https://doi.org/10.1016/j.epsl.2021.117014

Yokoo, S., Hirose, K., Sinmyo, R., & Tagawa, S. (2019). Melting experiments on liquidus phase relations in the Fe-S-O ternary system under core pressures.

Geophysical Research Letters, *46*, 5137–5145. https://doi.org/10.1029/2019GL082277

Yuan, L., & Steinle-Neumann, G. (2020). Strong sequestration of hydrogen into the Earth's core during planetary differentiation. *Geophysical Research Letters*, *47*, e2020GL088303. https://doi.org/10.1029/2020GL088303

References From the Supporting Information

Akahama, Y., & Kawamura, H. (2004). High-pressure Raman spectroscopy of diamond anvils to 250 GPa: method for pressure determination in the multimegabar pressure range. *Journal of Applied Physics*, *96*, 3748–3751. https://doi.org/10.1063/1.1778482

Badro, J., Siebert, J., & Nimmo, F. (2016). An early geodynamo driven by exsolution of mantle components from Earth's core. *Nature*, *536*, 326–328. https://doi.org/10.1038/nature18594

Caracas, R. (2015). The influence of hydrogen on the seismic properties of solid iron. *Geophysical Research Letters*, *42*, 3780–3785. https://doi.org/10.1002/2015GL063478

Chi, Z., Nguyen, H., Matsuoka, T., Kagayama, T., Hirao, N., Ohishi, Y., & Shimizu, K. (2011). Cryogenic implementation of charging diamond anvil cells with H_2 and D_2. *Review of Scientific Instruments*, *82*, 105109. https://doi.org/10.1063/1.3652981

Dewaele, A., & Torrent, M. (2013). Equation of state of α-Al_2O_3. *Physical Review B*, *88*, 064107. https://doi.org/10.1103/Physical Review B.88.064107

Dewaele, A. S., Loubeyre, P., Occelli, F., Mezouar, M., Dorogokupets, P. I., & Torrent, M. (2006). Quasihydrostatic equation of state of iron above 2 Mbar. *Physical Review Letters*, *97*, 215504. https://doi.org/10.1103/Physical Review Letters.97.215504

Dorogokupets, P. I., Dymshits, A. M., Litasov, K. D., & Sokolova, T. S. (2017). Thermodynamics and equations of state of iron to 350 GPa and 6000 K. *Scientific Reports*, *7*, 41863. https://doi.org/10.1038/srep41863

Helffrich, G. (2014). Outer core compositional layering and constraints on core liquid transport properties. *Earth and Planetary Science Letters*, *391*, 256–262. https://doi.org/10.1016/j.epsl.2014.01.039

Helffrich, G., Hirose, K., & Nomura, R. (2020). Thermodynamical modeling of liquid Fe-Si-Mg-O: molten magnesium silicate release from the core. *Geophysical Research Letters*, *47*, e2020GL089218. https://doi.org/10.1029/2020GL089218

Hirao, N., Kawaguchi, S. I., Hirose, K., Shimizu, K., Ohtani, E., & Ohishi, Y. (2020). New developments in high-pressure X-ray diffraction beamline for diamond anvil

cell at SPring-8. *Matter and Radiation at Extremes*, *5*, 018403. https://doi.org/10.1063/1.5126038

Hirose, K., Tagawa, S., Kuwayama, Y., Sinmyo, R., Morard, G., Ohishi, Y., & Genda, H. (2019). Hydrogen limits carbon in liquid iron. *Geophysical Research Letters*, *46*, 5190–5197. https://doi.org/10.1029/2019GL082591

Iizuka-Oku, R., Yagi, T., Gotou, H., Okuchi, T., Hattori, T., & Sano-Furukawa, A. (2017). Hydrogenation of iron in the early stage of Earth's evolution. *Nature Communications*, *8*, 14096. https://doi.org/10.1038/ncomms14096

Ikuta, D., Ohtani, E., Sano-Furukawa, A., Shibazaki, Y., Terasaki, H., Yuan, L., & Hattori, T. (2019). Interstitial hydrogen atoms in face-centered cubic iron in the Earth's core. *Scientific Reports*, *9*, 7108. https://doi.org/10.1038/s41598-019-43601-z

Ohta, K., Ichimaru, K., Einaga, M., Kawaguchi, S., Shimizu, K., Matsuoka, T., et al. (2015). Phase boundary of hot dense fluid hydrogen. *Scientific Reports*, *5*, 16560. https://doi.org/10.1038/srep16560

Seto, Y., Nishio-Hamane, D., Nagai, T., & Sata, N. (2010). Development of a software suite on X-ray diffraction experiments. *The Review of High Pressure Science and Technology*, *20*, 269–276

Figure 1. XRD patterns collected in (a) run #A4 for the Fe-O-H sample and (b) run #B for the Fe-H sample. Hcp, hcp FeH_x.; fcc, fcc FeH_x; dhcp, FeH; rB1, rhombohedral B1 FeO; cor, corundum (pressure medium); Re, rhenium (gasket). The bottom profile in (b) shows only peaks that appeared upon quenching temperature, which was used to calculate hydrogen concentration in liquid in run #B.

Figure 2. Sample cross sections and temperature profile in run #A4. Scanning ion microscope image (a) and X-ray map of oxygen (b) show that liquid coexisted with solid Fe and FeO. Crystals were formed from liquid upon quenching temperature, and their unit-cell volumes were used to calculate hydrogen concentration in liquid. Temperature at the liquid/solid boundary is obtained by a combination of these images and a temperature profile (c).

Figure 3. Liquidus phase diagrams of the Fe-FeO-FeH ternary system. Green lines are cotectic lines that separate the liquidus fields of Fe, FeO, and FeH. In (a) for ~40 GPa, diamond, circles, and square show the compositions of liquids coexisting with Fe, FeO and Fe + FeO, respectively (filled and open circle/square symbols indicate 0.1–0.4 wt% and 1.7 wt% C in liquids, respectively). The Fe-FeO eutectic liquid composition is given by a red triangle from Figure S1. The Fe-FeH eutectic liquid composition may be $FeH_{0.42}$ (Fe + 0.75 wt% H). (b) The liquidus phase relations extrapolated to 330 GPa considering the Fe-FeO (orange triangle, Figure S1) and Fe-FeH binary eutectic liquid compositions (the latter could exhibit little pressure dependence). The liquidus field of Fe at ICB conditions is illustrated by a blue area.

Figure 4. Possible ranges of the outer core liquid composition in the Fe-O-Si-H±1.7wt%S system. Colored areas show liquid compositions that are compatible with the observed outer core density and P-wave velocity (Umemoto & Hirose, 2020) and within the liquidus field of Fe. The areas enclosed by black lines indicate liquid compositions that are in equilibrium with the possible compositions of the inner core solid that explain observed density, P- and S-wave velocities (Li et al., 2018; Wang et al., 2021). If T_{CMB} is ~6000 K, the outer core may include ~3 wt% O and ~0.3 wt% H as important light elements.

Figure 1.

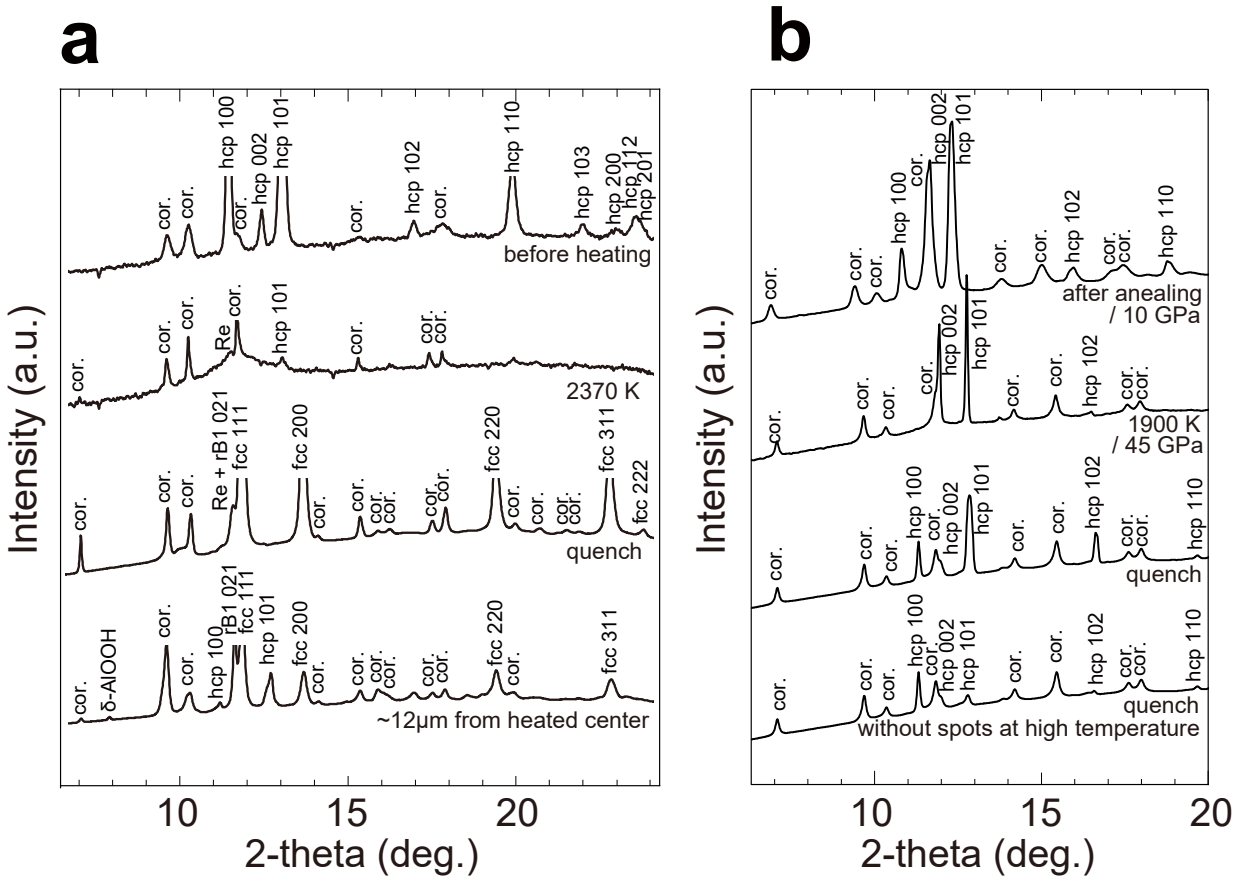
a
b
Intensity (a.u.)
2-theta (deg.)
10
15
20
cor.
δ-AlOOH
hcp 100
hcp 002
hcp 101
hcp 102
hcp 110
hcp 103
hcp 200
hcp 112
hcp 201
Re
Re + rB1 021
rB1 021
fcc 111
hcp 101
fcc 200
fcc 220
fcc 311
fcc 222
before heating
2370 K
quench
~12μm from heated center
after anealing
/ 10 GPa
1900 K
/ 45 GPa
quench
without spots at high temperature

Figure 2.

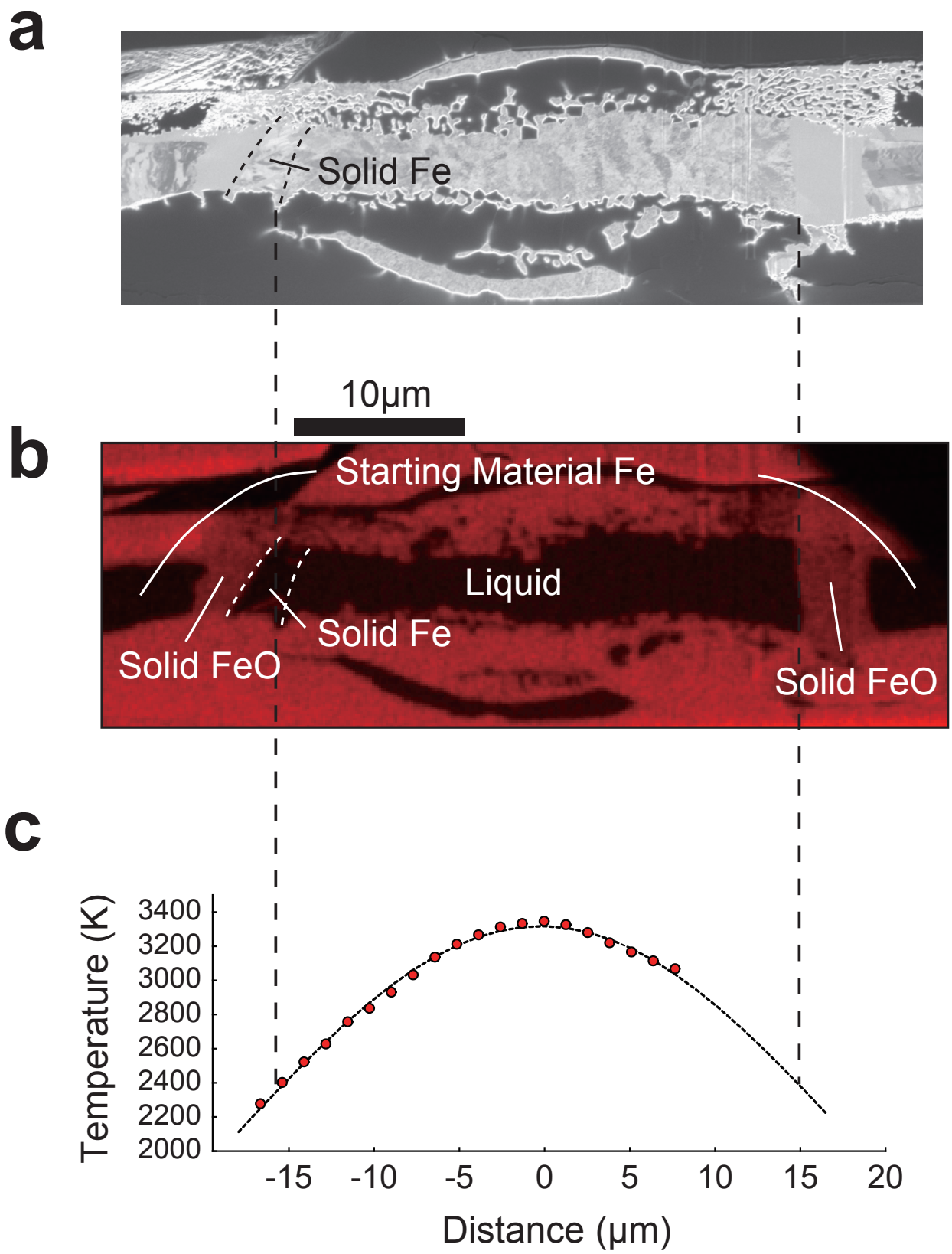
a
Solid Fe
10μm
b
Starting Material Fe
Liquid
Solid Fe
Solid FeO
Solid FeO
c
Temperature (K)
3400
3200
3000
2800
2600
2400
2200
2000
-15
-10
-5
0
5
10
15
20
Distance (μm)

Figure 3.

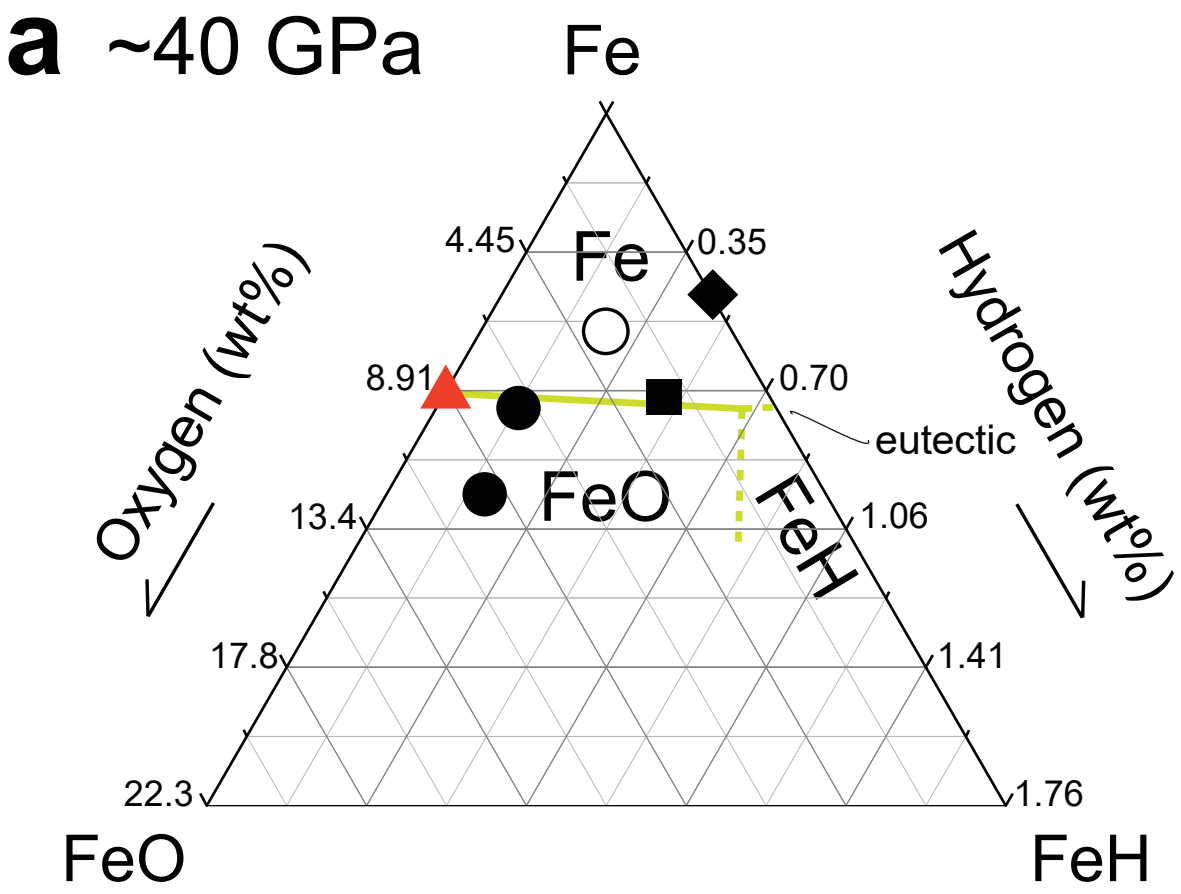
a ~40 GPa
Fe
4.45
0.35
Fe
8.91
0.70
eutectic
Oxygen (wt%)
Hydrogen (wt%)
FeO
13.4
1.06
FeH
17.8
1.41
22.3
1.76
FeO
FeH

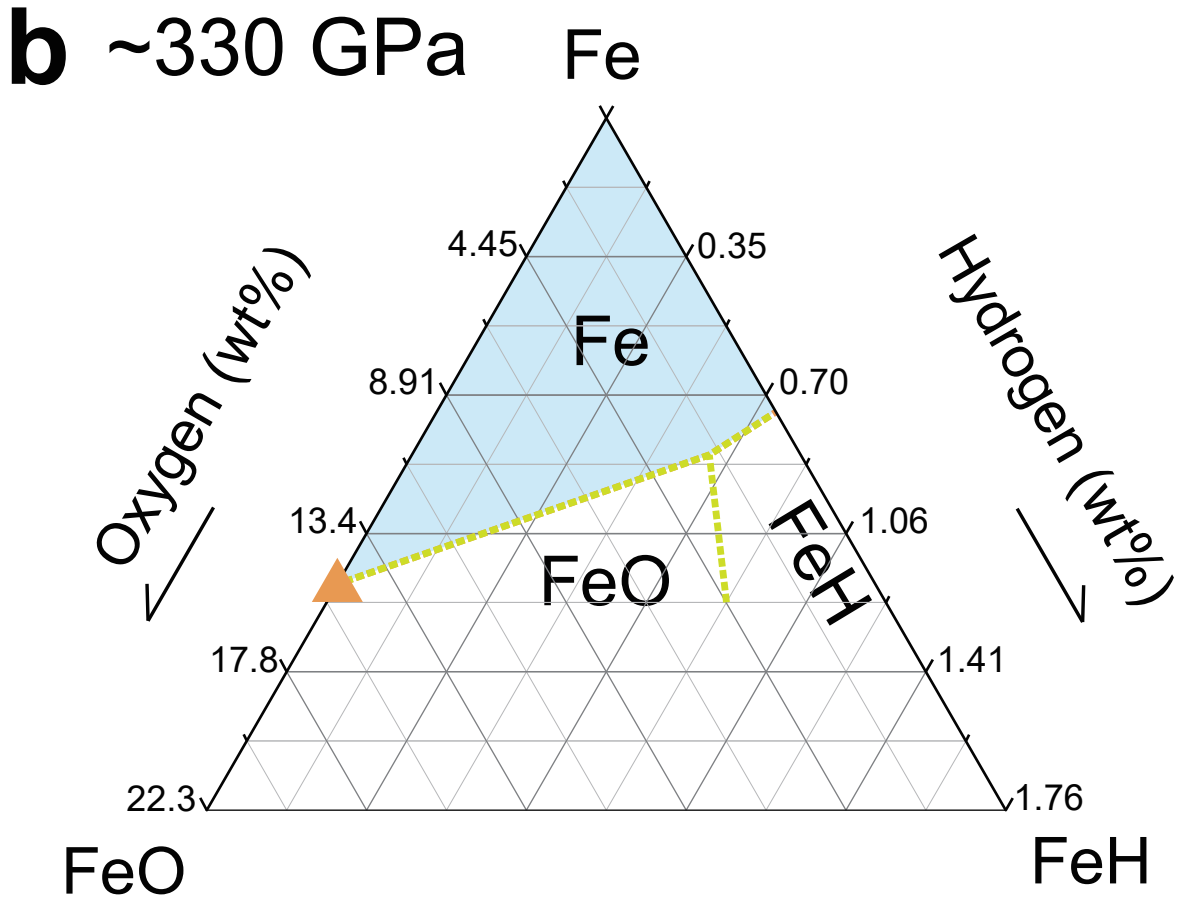
b ~330 GPa
Fe
4.45
0.35
Fe
8.91
0.70
Oxygen (wt%)
Hydrogen (wt%)
13.4
1.06
FeO
FeH
17.8
1.41
22.3
1.76
FeO
FeH

Figure 4.

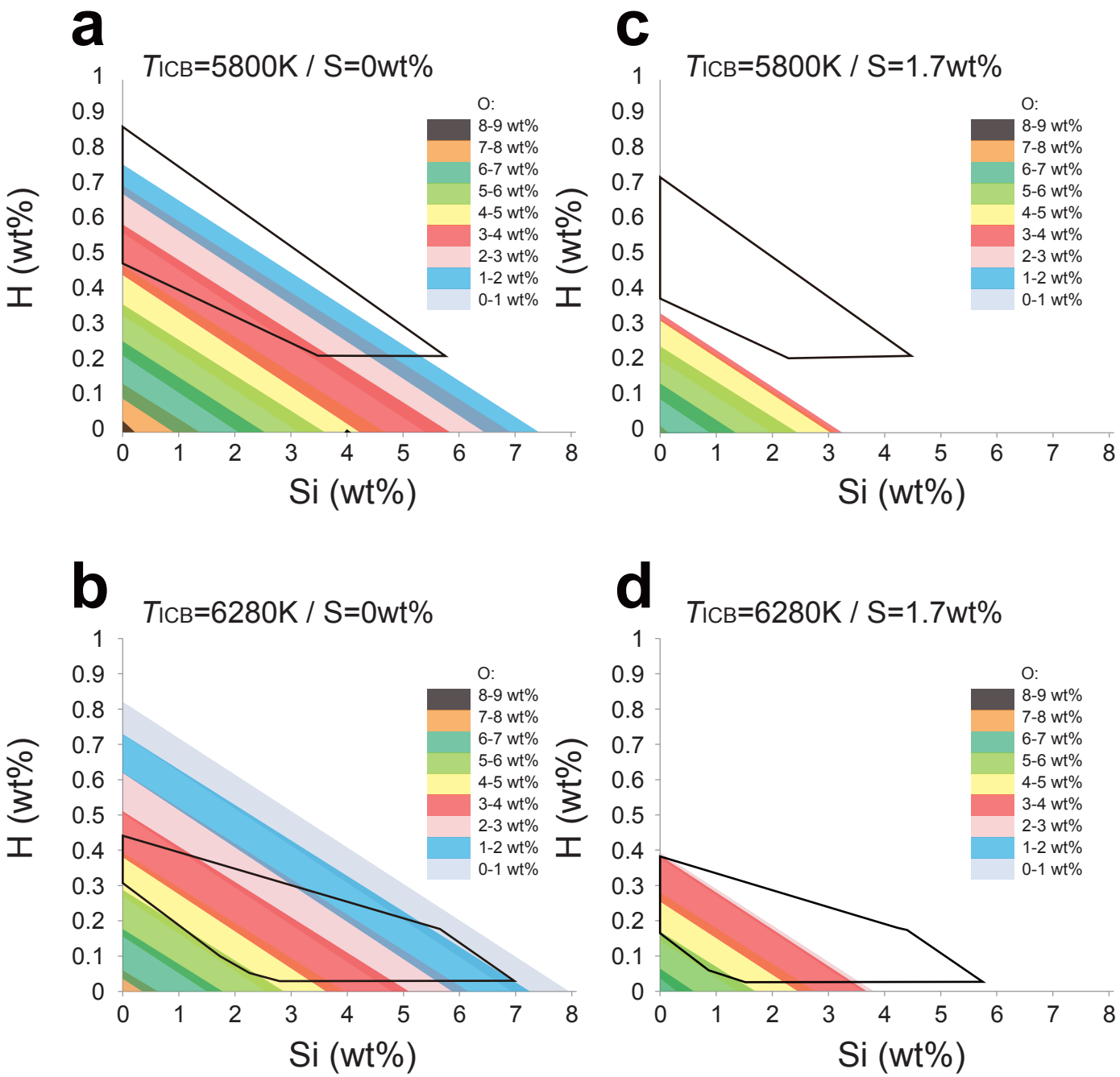
a
TICB=5800K / S=0wt%
c
TICB=5800K / S=1.7wt%
b
TICB=6280K / S=0wt%
d
TICB=6280K / S=1.7wt%
H (wt%)
Si (wt%)
O:
8-9 wt%
7-8 wt%
6-7 wt%
5-6 wt%
4-5 wt%
3-4 wt%
2-3 wt%
1-2 wt%
0-1 wt%

Geophysical Research Letters

Supporting Information for

Melting Experiments on Fe-O-H and Fe-H: Evidence for Eutectic Melting in Fe-FeH and Implications for Hydrogen in the Core

Kenta Oka[1], Nagi Ikuta[1], Shoh Tagawa[1,2], Kei Hirose[1,2], and Yasuo Ohishi[3]

[1]Department of Earth and Planetary Science, The University of Tokyo, Bunkyo, Tokyo, Japan

[2]Earth-Life Science Institute, Tokyo Institute of Technology, Meguro, Tokyo, Japan

[3]Japan Synchrotron Radiation Research Institute, SPring-8, Sayo, Hyogo, Japan

Contents of this file

Experimental Methods

Melting experiments on the Fe-O-H system. We used diamond anvils with flat 300 μm or single-beveled 120 μm culet size for experiments on Fe-O±H (Table S1). A pure Fe (5N, *Mairon-UHP*, *Toho Zinc*) or Fe-12wt%O foil, same as that used in Oka et al. (2019), was loaded into a hole at the center of a pre-indented rhenium gasket, together with a powder mixture of $Al(OH)_3$ and Al_2O_3 (a source of oxygen and hydrogen) and 10 μm-thick Al_2O_3 sapphire single crystals (thermal insulation layers). Upon heating, $Al(OH)_3$ dehydrates to form AlOOH or Al_2O_3. The mixing ratio between Al_2O_3 and $Al(OH)_3$ was varied in order to change the Fe/H_2O ratio of a system.

The sample was heated from both sides with a couple of 100W single-mode Yb fiber lasers with flat-top beam-shaping optics. The laser spot size was 20–30 μm across. The heating duration was limited to less than 3 sec to avoid temperature fluctuations which could lead to a complex melting texture. Indeed, it is long enough for O and H to diffuse over a melt pocket (Helffrich, 2014), which assures chemical equilibrium between liquid and solid when considering that melting/crystallization at the liquid-solid boundary occurs almost instantaneously (Yokoo et al., 2019; Hasegawa et al., 2021). According to previous time-series melting experiments on the Fe-S system, the compositions of coexisting liquid and solid did not change after heating for 1 sec in a laser-heated DAC (Mori et al., 2017). The diffusivities of O and H in molten iron are higher than that of S (Helffrich, 2014). A temperature profile was obtained using a spectro-radiometric method (Hirao et al., 2020). The temperature at the liquid/solid boundary corresponds to the liquidus temperature of a liquid obtained in each run. We determined it by combining the temperature profile with a sample cross-section (e.g., Mori et al., 2017; Tateno et al., 2018; Oka et al., 2019) (Figure 2c).

We performed XRD measurements in-situ at high *P*-*T* using an X-ray beam with energy of ~30 keV at the beamline BL10XU, SPring-8 (Figure 1). XRD spectra were collected on a flat panel detector (FPD, *Perkin Elmer*) with exposure time of 1 sec before and after heating at 300 K and of 0.2 sec continuously during laser heating. The IPAnalyzer software (Seto et al., 2010) was used to integrate two-dimensional XRD image into one-dimensional diffraction profile. Sample pressure was measured at 300 K after heating based on the unit-cell volume of Al_2O_3 corundum and its equation of state (Dewaele & Torrent, 2013). We considered that 60% and 90% of theoretical thermal pressure for purely isochoric heating, $\Delta P = \alpha K_T \times (T - 300)$ ($\alpha K_T = 4$ and 9 MPa/K), contributed to an increase in sample pressure during heating at ~40 GPa and ~150 GPa, respectively (e.g., Hirose et al., 2019; Oka et al., 2019).

Textural and chemical characterizations except for H (see below) were carried out on each recovered sample; it is well known that H escapes from metal Fe when it transforms into bcc during decompression (e.g., Iizuka-Oku et al., 2017; Tagawa et al., 2021). A sample cross-section and X-ray elemental maps were obtained parallel to the compression axis by a focused ion beam (FIB, *FEI Versa 3D DualBeam*) and an energy-dispersive spectroscopy (EDS) attached to a field-emission (FE)-type scanning electron microscope (SEM) (Figures 2a, b). Quantitative chemical analyses were then made for coexisting liquid and crystals (liquidus phases) with an FE-type electron probe micro-analyzer (FE-EPMA, *JEOL JXA-8530F*) with an accelerating voltage of 12 kV, a current of 15 nA, and the X-ray counting time of 20/10 sec for peak/background. Fe, Fe_3C, and corundum were used as standards. LIF (Fe), LDE2H (C), TAP (Al), and LDE1 (O) were analyzing crystals. The FE-EPMA analyses of quenched liquid Fe sometimes included a small amount of Al, which is likely a signal from the surrounding pressure medium or Al_2O_3 grains that mechanically intruded into the liquid; note that the amount of Al incorporated into liquid Fe metal is negligible (Badro et al., 2016; Helffrich et al., 2020). Al was therefore subtracted as Al_2O_3 from raw data. C was detected not only in the quenched liquid but also inside the rhenium gasket; the latter could be due to contamination during FIB and/or FE-EPMA analysis. Thus, we subtracted 0.2–0.4 wt% C from the raw analyses of liquids, which was found on the rhenium gasket in the same sample cross-section. The liquid should have included the remaining 0.1–3.7 wt% C (Table S1).

H concentration, x in FeH_x, was estimated from its lattice volume (Hirose et al., 2019; Tagawa et al., 2021), which expands proportionally to the H content (Caracas, 2015);

$$x = \frac{V_{FeHx} - V_{Fe}}{\Delta V_H}, \quad (1)$$

where V_{FeHx} and V_{Fe} are the unit-cell volumes of FeH_x and Fe (Dorogokupets et al., 2017 for fcc Fe and Dewaele et al., 2006 for hcp Fe), respectively, and ΔV_H is an increase in the lattice volume of Fe per H atom from Caracas (2015). Note that theoretically-derived ΔV_H for the hcp phase at 0 K by Caracas (2015) is quite consistent with the room-temperature ΔV_H obtained experimentally for fcc by Tagawa, Gomi et al. (2022). The error in the H content, x, is estimated to be ±8% at maximum, which is mainly derived from uncertainty in ΔV_H (Ikuta et al., 2019; Tagawa et al., 2021).

Melting experiment on the Fe-H system. We have also conducted a melting experiment on the Fe-FeH binary system (Table S2), using a laser-heated DAC with beveled 200 μm culet anvil. A 10-μm thick pure iron foil was loaded between the pellets

of Al_2O_3 powder. A whole DAC was dried in a vacuum oven at 393 K for at least 1 hr and subsequently at 350 K for 30 min in a vacuumed hydrogen-loading system.

Hydrogen was cryogenically loaded into a sample chamber (Chi et al., 2011). After the chamber was filled with liquid hydrogen, sample was compressed at ~15 K and then restored to room temperature. The surface of the diamond anvils was coated with a thin layer of Ti by sputtering (Ohta et al., 2015) in order to avoid anvil failure. We synthesized the FeH_x sample at 10 GPa and melted it at 45 GPa with in-situ XRD measurements at BL10XU, SPring-8 (Figure 1b). We obtained pressures from the Raman shift of a diamond anvil (Akahama & Kawamura, 2004) and from the lattice volume of Al_2O_3 corundum when XRD data were available (Dewaele & Torrent, 2013). The temperature at the liquid/solid boundary was found to be 1900 K in the temperature profile considering the width of a liquid pool estimated by scanning the sample with respect to an X-ray beam. Other procedures including the determination of the H contents in solid and liquid Fe phases were similar to those for the Fe-O±H sample described above.

Table S1

Experimental Results on the Fe-O±H System

Run #	Starting materials	P (GPa) at high T	P (GPa) at 300 K	T (K)	Liquid composition			Liquidus phase
					O (wt%)	H (wt%)	C (wt%)	
A1	Fe-12wt%O + Al_2O_3 + $Al(OH)_3$[a]	35(2)	30(2)	2460(120)	3.53(4)	0.27(2)	1.68(9)	FeO
A2	Fe-12wt%O + Al_2O_3 + $Al(OH)_3$[b]	37(2)	32(2)	2470(110)	7.20(4)	0.18(1)	0.11(9)	FeO
A3	Fe-12wt%O + Al_2O_3 + $Al(OH)_3$[b]	41(2)	36(2)	2400(120)	9.53(18)	0.22(2)	0.20(12)	FeO
A4	Fe + $Al(OH)_3$	39(2)	33(2)	2370(120)	2.98(29)	0.49(4)	0.43(4)	Fe[d] + FeO
A5	Fe + Al_2O_3 + $Al(OH)_3$[c]	147(15)	122(12)	3200(320)	12.97(86)	0.00(0)	0.86(7)	Fe
A6	Fe + Al_2O_3 + $Al(OH)_3$[c]	160(16)	136(14)	3200(320)	10.36(56)	0.04(0)	3.74(23)	FeO

[a] Al_2O_3 : $Al(OH)_3$ = 10 : 3 by weight

[b] Al_2O_3 : $Al(OH)_3$ = 10 : 4 by weight

[c] Al_2O_3 : $Al(OH)_3$ = 10 : 8 by weight

[d] contains 0.43(3) wt% H calculated from its unit-cell volume of 20.5 $Å^3$

Table S2

Experimental Results on the Fe-H System

Run #	P (GPa)	T (K)	solid hcp-FeHx				quenched liquid hcp-FeHx			
			a (Å)	c (Å)	V ($Å^3$)	x	a (Å)	c (Å)	V ($Å^3$)	x
B	10(1)	300	2.528(1)	4.067(3)	22.51(8)	0.30(2)				
	45(2)	1900(100)	2.426(5)	3.969(7)	20.23(24)					
	41(2)	300	2.422(0)	3.894(1)	19.78(3)	0.20(2)	2.418(2)	3.948(5)	20.00(13)	0.26(2)

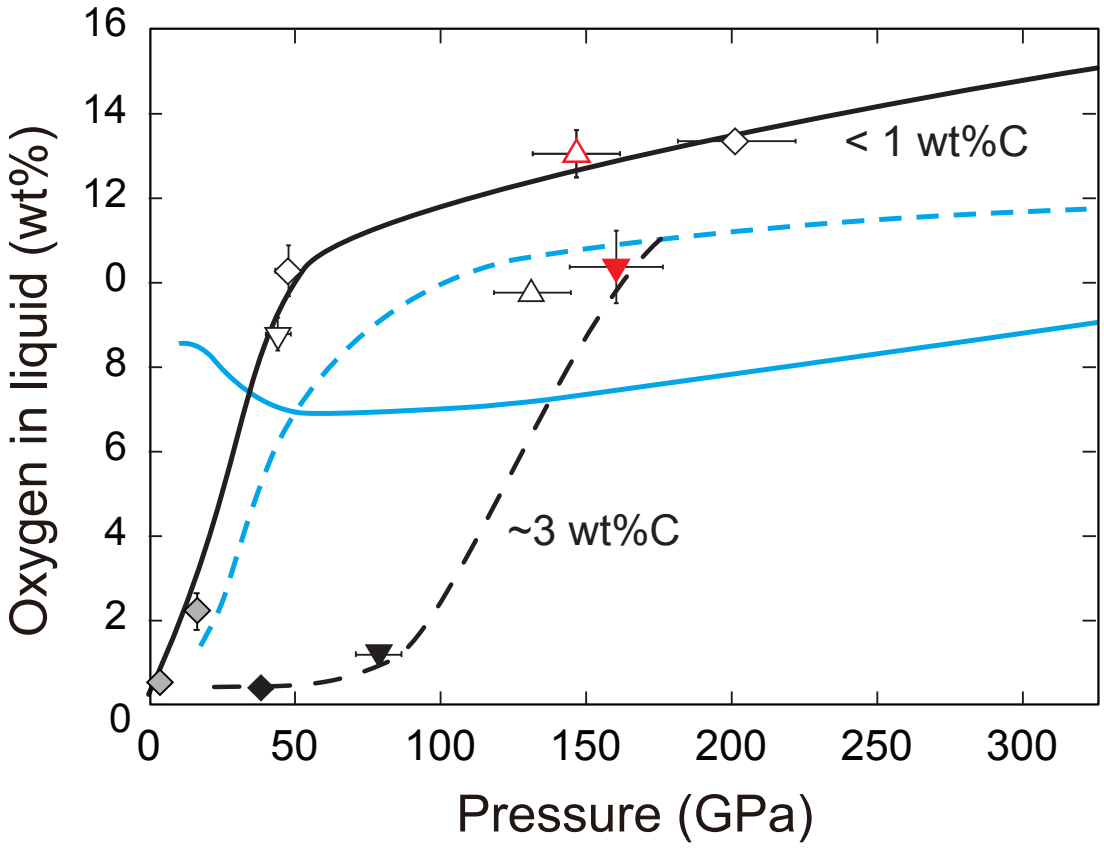

Figure S1. Liquid compositions obtained in melting experiments on the Fe-FeO±C system. Normal and reverse triangles, lower and upper bounds for O concentration in the Fe-FeO eutectic liquid, respectively; diamonds, the O contents in liquids coexisting both Fe and FeO (eutectic liquids). Red, this study (runs #A5 and #A6); black, Oka et al. (2019); gray, Ohtani et al. (1984) and Ringwood & Hibberson (1990). The black curves indicate changes in O concentration in liquids coexisting with Fe and FeO (solid line, with <1 wt% C in liquids; broken line, with ~3 wt% C in liquids). Blue dashed and solid curves represent thermodynamically-modelled eutectic liquid compositions in the Fe-FeO system assuming non-ideal and ideal solutions, respectively (Komabayashi, 2014).